Ocean Heat Transport, Sea Ice, and Multiple Climate States: Insights from Energy Balance Models

BRIAN E. J. ROSE AND JOHN MARSHALL

Department of Earth, Atmospheric, and Planetary Sciences, Massachusetts Institute of Technology, Cambridge, Massachusetts

(Manuscript received 17 December 2008, in final form 5 March 2009)

ABSTRACT

Several extensions of energy balance models (EBMs) are explored in which (i) sea ice acts to insulate the atmosphere from the ocean and (ii) ocean heat transport is allowed to have some meridional structure controlled by the wind, with minima at which the ice edge can rest. These new models support multiple stable ice edges not found in the classical EBM and a hysteresis loop capable of generating abrupt warming as the ice edge ''jumps'' from mid- to high latitudes. The new equilibria are demonstrated in two classes of model, in which the wind stress is either specified externally or generated interactively. Wind stress is computed by introducing a dynamical constraint into the EBM to represent the simultaneous meridional transport of energy and angular momentum in the atmosphere. This wind stress is used to drive ocean gyres, with associated structure in their meridional heat transport, so that the atmosphere and ocean are coupled together both thermally and mechanically.

1. Introduction

The use of simple one-dimensional heat balance equations to study the climate system, and in particular the effects of heat transport and ice–albedo feedback, goes back to Budyko (1969) and Sellers (1969). Important contributions to the theory of energy balance models (EBMs) were made by, notably, Held and Suarez (1974), North (1975a,b), and Lindzen and Farrell (1977, 1980). A thorough review of this classic literature is given by North et al. (1981). These simple models provide an elegant illustration of the ice–albedo feedback. Typically, the surface temperature is set by the competing effects of transport and radiation, while the ice cover (which sets the albedo and thus exerts a powerful control on the radiation budget) is determined by a simple threshold condition on the surface temperature. One of the hallmarks of this nonlinear interaction is the existence of at least two vastly different climates for a given solar forcing: a moderate climate with a small ice cap or no ice and a very cold, completely ice-covered climate (which we will refer to as the ''snowball'' state). Graphs of the ice edge versus solar constant appear in all the above-cited classic EBM papers to illustrate the multiple-valued structure of the solutions. Between the two stable equilibria lies a third solution with a large but finite ice cover. However, this large ice cap is unstable to small perturbations and is thus not a physically realizable state.

In contrast, in this paper we present a new model that supports multiple stable ice edges: a moderate climate with high-latitude ice and a colder climate with a midlatitude ice edge. We develop the new model in a series of extensions of the basic EBM, illustrating at each step how the relationship between ice edge and solar forcing changes. Sketches of the models can be found in Figs. 1–4. As we will show, two new pieces of physics are critical to the existence of a stable midlatitude ice edge. First, the ice (which here we suppose is sea ice) must be allowed to insulate the ocean from the atmosphere. Second, the ocean heat transport must exhibit some latitudinal structure with minima at which the ice edge is found to rest. We will discuss how such structure in ocean meridional energy transport might be expected to naturally arise as a consequence of, for example, wind-driven ocean gyres.

The atmosphere and ocean play different roles in setting the sea ice edge. Studies of the modern climate indicate that the spatial distribution of ocean heat transport

Corresponding author address: Brian Rose, Department of Earth, Atmospheric, and Planetary Sciences, MIT, 54-1419, 77 Massachusetts Ave., Cambridge, MA 02139.
E-mail: brose@mit.edu

DOI: 10.1175/2009JAS3039.1

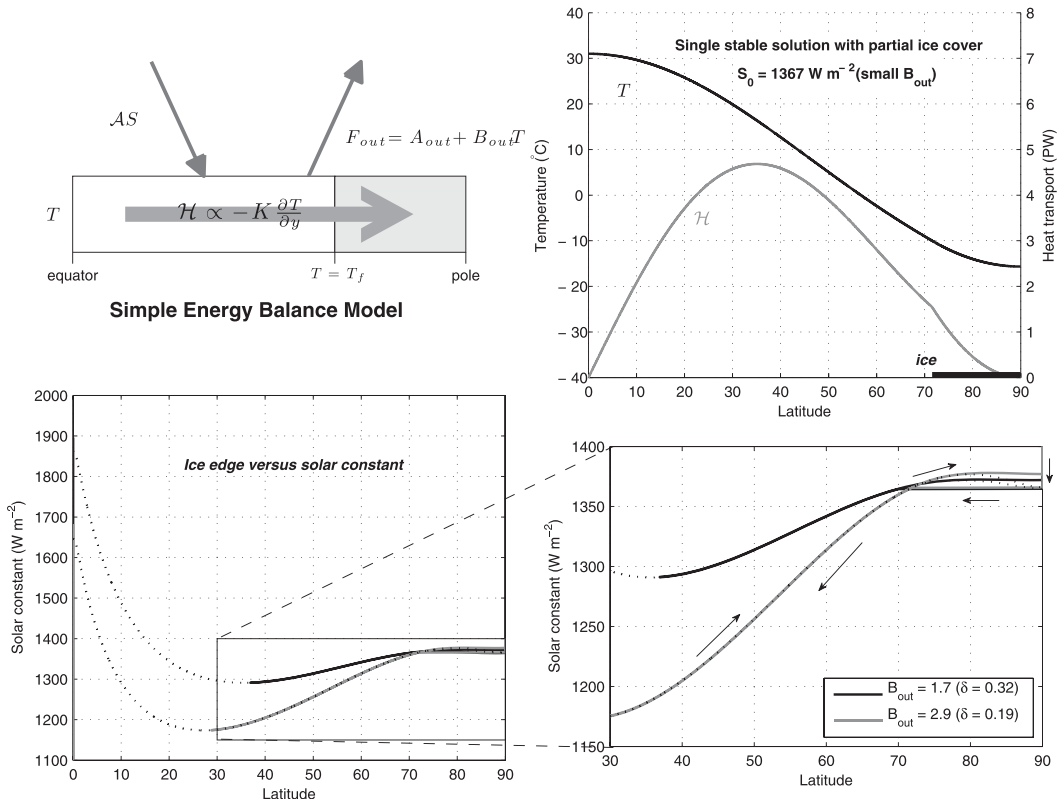

FIG. 1. The classic diffusive energy balance model, (top left) illustrated in a schematic (thin gray arrows represent radiative fluxes; thick gray arrow represents poleward energy transport due to atmospheric and oceanic circulation, which is parameterized as a diffusive process). (top right) Temperature and heat transport are plotted as functions of latitude for a particular numerical solution of (1). (bottom left) We plot S_0 vs ice edge ϕ_i for two different parameter sets yielding different sensitivities ($\delta = 0.32$ in black and $\delta = 0.19$ in gray; see Table 1 for all parameter values). Multiple equilibria for a given S_0 can be read horizontally in these plots. The dashed curves show the analytic steady-state solution of (1) (adapted from North 1975a), including the unstable low- and high-latitude branches. The solid curves show the equilibrated numerical solutions of the time-dependent system (stable states only). (bottom right) An expanded view of the stable finite ice cover solutions. The small arrows indicate the path taken by the numerical integration; the small ice cap instability is evident poleward of about 80°.

convergence is the most important factor setting the observed sea ice margin (Bitz et al. 2005). Recent work on modeling the Neoproterozoic snowball earth has also emphasized the critical role of ocean heat transport in limiting sea ice expansion in radically different climates (e.g., Poulsen et al. 2001; Bendtsen 2002; Lewis et al. 2003; Poulsen and Jacob 2004; Donnadieu et al. 2004). Recognition that the stability of the climate system in the face of the ice–albedo feedback might be better modeled by treating the atmosphere and ocean separately in simple models goes back at least to Held and Suarez (1974). Although there have been numerous simple model studies of interactions between sea ice and ocean thermohaline circulation (e.g., Yang and Neelin 1993, 1997; Nakamura 1996; Jayne and Marotzke 1999; Bendtsen 2002), there has been relatively little attempt to represent the wind-driven component of the ocean heat transport in such models, despite evidence from fully coupled GCMs that the wind-driven circulation is the most important barrier to sea ice expansion into the low latitudes in the approach to the snowball earth (Poulsen and Jacob 2004). Idealized models of the wind-driven ocean heat transport have been explored by Klinger (1996), Wang et al. (1995), Klinger and Marotzke (2000), Cessi (2000), Gallego and Cessi (2000), Primeau and Cessi (2001), and Hazeleger et al. (2004), among others. Our goal here is to explore the interaction of the wind-driven ocean heat transport with sea ice–albedo feedback in the framework of an EBM.

Our paper is organized as follows: in section 2 we briefly review aspects of traditional EBMs (Fig. 1), and we take the first step in our extension of them by introducing distinct representations of the atmosphere and ocean (Fig. 2). In section 3 we consider refinements that attempt to more completely capture the role of meridional structure in ocean circulation and energy

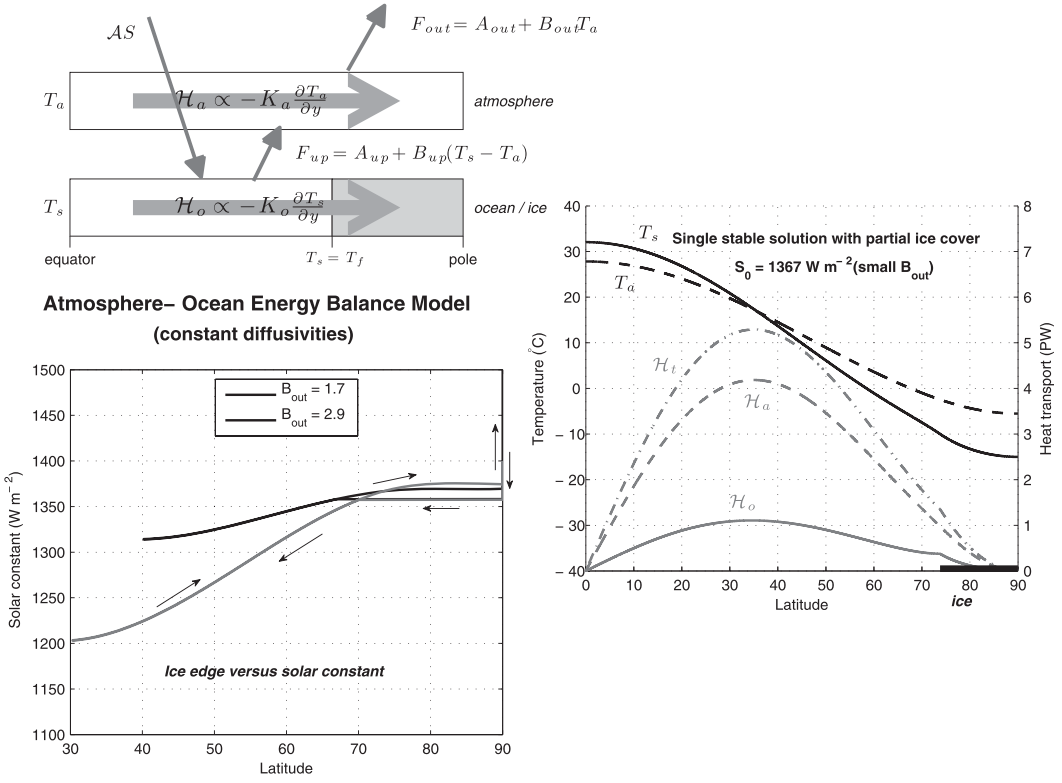

FIG. 2. As in Fig. 1, but for the atmosphere–ocean EBM, Eq. (5), with constant diffusivities K_a, K_o. (right) meridional profiles of T_a, T_s, $\mathcal{H}_t$, $\mathcal{H}_a$, and $\mathcal{H}_o$ together with the ice edge are shown. Note that the use of constant K_o allows for significant ocean heat transport poleward of the ice edge, which cannot, therefore, be insulating. (bottom left) We plot S_0 vs ϕ_i for this system (only stable solutions, obtained numerically, are shown). The path taken by the numerical integration is again illustrated by the small arrows.

transport in setting the ice edge. The resulting model is illustrated in Fig. 3. We show how the inclusion of additional physics, built into the EBM by allowing the ocean diffusivity to vary with latitude, leads to the new stable equilibrium with a large, finite ice cover. In section 4 we present a significant extension of the EBM hierarchy in which we attempt to capture not only meridional energy transport by the atmosphere but also its angular momentum transport, allowing one to infer patterns of surface winds and thence wind-driven ocean circulation and its associated energy transport. The resulting energy-momentum balance model, which is shown in Fig. 4, couples the atmosphere and ocean both dynamically and thermodynamically and also supports a large finite ice sheet as a stable solution. We present conclusions in section 5.

2. Diffusive energy balance models

a. Brief review of some classic EBM results

Our new model will be developed as an explicit generalization of the classic one-dimensional hemispheric diffusive EBM, which we now therefore briefly review. This model is illustrated in schematic form at the top left of Fig. 1. To help situate our discussion and introduce notation, we now write down an equation for this well-known model:

$$C_a \frac{\partial T_a}{\partial t} = D_y\left(C_a K_a \frac{\partial T_a}{\partial y}\right) + \mathcal{A}S - B_{\text{out}} T_a - A_{\text{out}}, \qquad (1)$$

where T_a is the surface air temperature, $\mathcal{A}$ is the coalbedo, S is the latitudinal distribution of incident solar radiation, $A_{\text{out}} + B_{\text{out}}T_a$ is the outgoing longwave radiation (OLR), C_a (J m^{-2} °C^{-1}) is a heat capacity for the column, K_a (m^2 s^{-1}) is a large-scale diffusivity, and D_y is an operator representing the meridional divergence (all quantities represent zonal averages).[1] This equation is readily derived from a zonally averaged and

[1] In (1) and what follows, we express the meridional component of the divergence in terms of the operator $D_y[h(\phi)] = (a\cos\phi)^{-1}\partial/\partial\phi[\cos\phi h(\phi)]$ for any function $h(\phi)$, where ϕ is latitude and a is the planetary radius. This operator simplifies the notation while including the necessary spherical geometric factors. Gradients are expressed in terms of a dimensional variable $dy = a\,d\phi$.

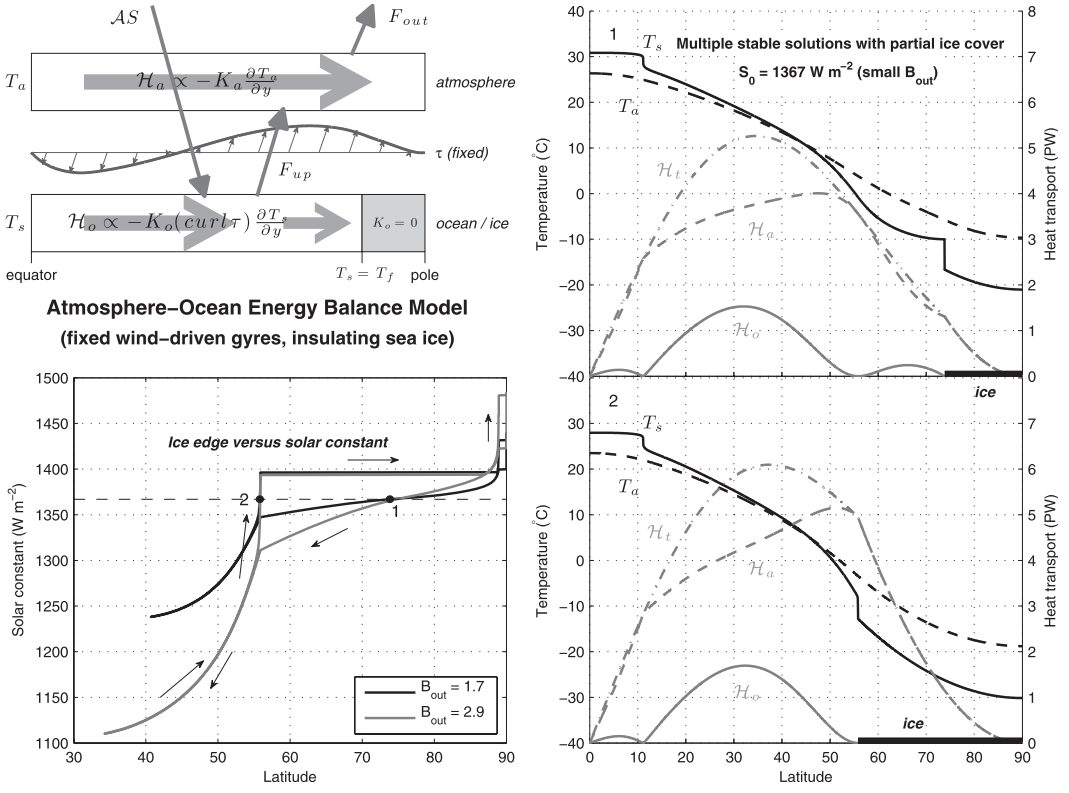

FIG. 3. As in Fig. 2, but for the AO-EBM (5) with latitudinal structure in the ocean diffusivity K_o. A prescribed wind stress (taken from Fig. 4) is used to drive ocean gyres through the parameterization (11). Here K_o is set to zero under the ice to account for the insulating effect of sea ice. The gyre model gives a bimodal ocean heat transport with a minimum at the midlatitude zero curl line. This leads to qualitatively different behavior of the ice edge compared to the simple EBM. Two stable ice edges are found for a range of S_0 values: (top right) one moderate solution with partial ice cover over the subpolar gyre (solution 1) and (bottom right) one cold solution with a completely ice-covered subpolar gyre (solution 2). (bottom left) The S_0–ϕ_i curves for this model. The small arrows at lower left again indicate the path taken by the ice edge in numerical integrations.

column-averaged heat budget for the climate system, with parameterizations relating the radiation, transport, and albedo as functions of T_a. Note that in this simplest of EBMs there is no attempt to represent atmospheric and oceanic heat transport separately.

Our calculations use the following:

$$S = \frac{S_0}{4}[1 + s_2 P_2(\sin\phi)], \tag{2a}$$

$$\mathcal{A} = \begin{cases} \mathcal{A}_o, & \text{for} \quad T_a > T_f, \\ \mathcal{A}_i, & \text{for} \quad T_a \le T_f, \end{cases} \quad \text{and} \tag{2b}$$

$$\mathcal{A}_o = a_0 + a_2 P_2(\sin\phi). \tag{2c}$$

Equation (2a) is a reasonable approximation to the observed annual mean distribution of solar radiation, where $P_2(x) = (3x^2 - 1)/2$ is the second Legendre polynomial, $s_2 = -0.48$, and S_0 is the solar constant (W m^{-2}). Equation (2b) is the crucial representation of the ice–albedo feedback, with the threshold temperature T_f typically taken to be -10°C [based on the observed annual mean snow and ice line, going back to Budyko (1969)]. Equation (2c) is a formula from North (1975b) designed to account crudely for observed changes in cloudiness and solar zenith angle with latitude. Detailed justification for these parameterizations can be found in North et al. (1981) and references therein.

We have followed Sellers (1969) in representing meridional heat transport $\mathcal{H}$ as a diffusive process directed down the mean temperature gradient. This is one of two classes of parameterizations used for $\mathcal{H}$ in the EBM literature. The other, going back to Budyko (1969), is slightly more convenient mathematically but provides a less clear connection to the more sophisticated models considered later in this paper.

When K_a is constant, the steady-state form of (1) has known analytic solutions (e.g., North 1975a; Held and Suarez 1974). The crucial nondimensional parameter for these models can be written as

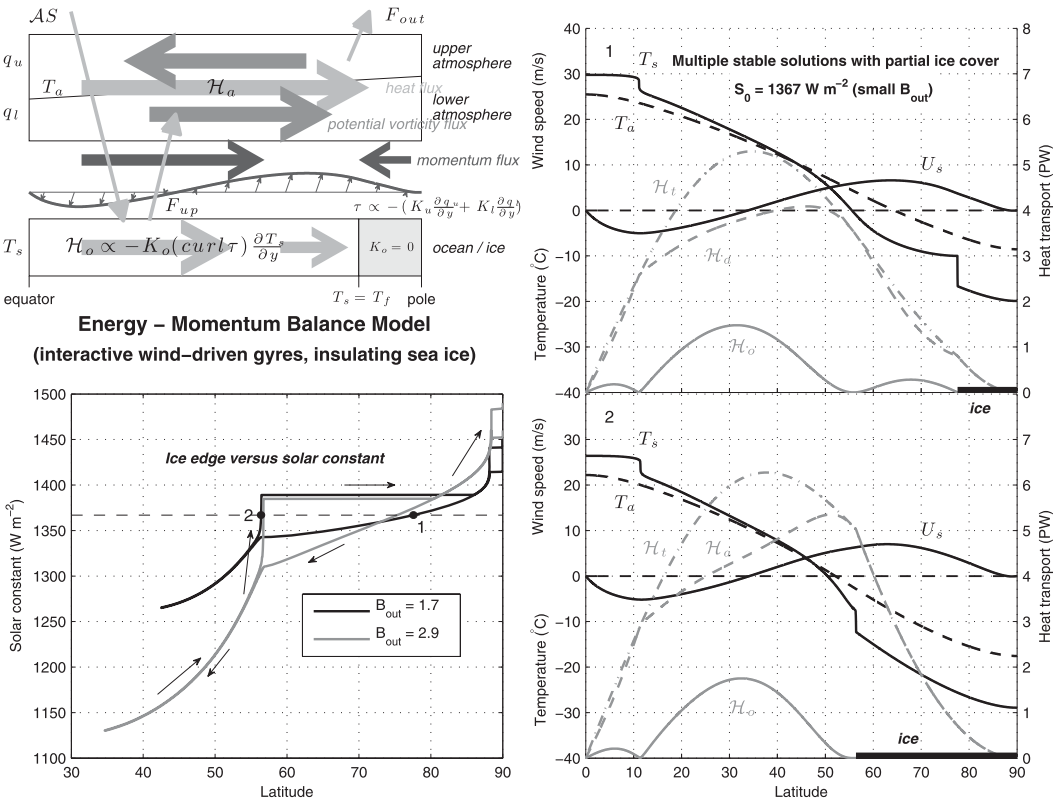

FIG. 4. Solutions from the energy-momentum balance model. The atmosphere is now represented by two layers of QGPV [Eq. (13)], with the temperature T_a in thermal wind balance with the vertical wind shear. Meridional fluxes of heat and angular momentum (sketched in light and dark gray respectively) are implicitly represented by a meridional eddy QGPV flux (sketched in medium gray). The ocean is driven by τ, generated interactively by the atmospheric model (the westerlies being maintained by the convergence of momentum fluxes in midlatitudes); otherwise the ocean is identical to that shown in Fig. 3. The model supports multiple stable ice edges, as illustrated in the top right and bottom right. The $S_0 - \phi_i$ relationships (lower left) are similar to those in the AO-EBM with fixed wind-driven gyres (Fig. 3).

$$\delta = \frac{C_a K_a}{B_{\text{out}} a^2}, \tag{3}$$

which is the ratio of radiative (C_a/B_{out}) to dynamical (a^2/K_a) time scales; it measures the efficiency of the poleward heat transport (Stone 1978).[2] Held and Suarez (1974) discuss in detail how the sensitivity of the ice edge to changes in the radiative budget increases with δ. We confirm this by plotting the equilibrium ice edge (at latitude ϕ_i) versus solar constant S_0 for $\delta = 0.32$ and $\delta = 0.19$. The analytic solutions are plotted as dashed lines in the lower panels of Fig. 1; the value of δ determines the slope of these curves (the sensitivity of the ice edge) but does not alter the qualitative behavior of the system.

The S_0 versus ice edge curves in Fig. 1, which for brevity will henceforth be referred to as ϕ_i–S_0 curves, illustrate the well-known multiple-equilibrium property of the EBM: for a given S_0, there may be anywhere from one to five different values of ϕ_i that solve (1) exactly. The regions of the graph where $dS_0/d\phi_i < 0$ are unstable (Cahalan and North 1979) and thus physically are unrealizable. The ''large ice cap instability'' occupies the subtropical and tropical latitudes; an ice margin within these latitudes expands rapidly toward the equator. The ''small ice cap instability'' (SICI) occupies the polar latitudes. A very small amount of polar ice must either melt completely or grow to a minimum stable size. There is thus a range of solar constants over which a total of three stable solutions coexist: ice-free, moderate ice cap, and snowball. Discussions of SICI and its physical mechanism are given by Held and Suarez (1974), Lindzen and Farrell (1977), and North (1984). The minimum stable ice cap size is proportional to δ (as can be seen in Fig. 1)

[2] This parameter is called D in North's papers. The equivalent parameter for the Budyko-type EBM is called δ by Held and Suarez (1974).

TABLE 1. Parameter values used for the numerical solutions of the four classes of models. In each case two solutions are computed, using two sets of values for the longwave cooling A_{out}, B_{out} as shown. The dash (—) indicates unitless parameters or parameters that are not used in particular models.

Parameter	Units	EBM Fig. 1	AO-EBM (constant K_o) Fig. 2	AO-EBM (fixed wind) Fig. 3	EMomBM Fig. 4
a	m	6.373×10^6	same	same	same
T_f	°C	−10	same	same	same
s_2	—	−0.48	same	same	same
a_0	—	0.70	same	same	same
a_2	—	−0.078	same	same	same
$\mathcal{A}_i$	—	0.38	same	same	same
C_a	J m^{-2} °C^{-1}	10^7	same	same	same
C_o	J m^{-2} °C^{-1}	—	10^7	same	same
K_a	m^2 s^{-1}	2.2×10^6	2.7×10^6	2.7×10^6	—
K_o	m^2 s^{-1}	—	5.2×10^5	—	—
B_{up}	W m^{-2} °C^{-1}	—	15	same	same
A_{up}	W m^{-2}	—	238	same	same
B_{out}	W m^{-2} °C^{-1}	2.9/1.7	2.9/1.7	2.9/1.7	2.9/1.7
A_{out}	W m^{-2}	207/212	199/211	208/217	205/216
R	J kg^{-1} °C^{-1}	—	—	—	287
ϵ	kg m^{-2} s^{-1}	—	—	—	0.04
k_l	m^2 s^{-1}	—	—	—	6×10^6
L_d	m	—	—	—	5×10^5
μ	m^3 kg^{-1} °C^{-1}	—	—	—	350

and represents the minimum distance over which the temperature (and thus the outgoing radiation) can adjust locally to the albedo forcing of the ice cap—shorter length scales are wiped out by diffusion. SICI has been explored in both EBMs and more comprehensive climate models by Huang and Bowman (1992), Matteucci (1993), Lee and North (1995), Maqueda et al. (1998), and Langen and Alexeev (2004), among others. SICI is far from universal in climate models, however, as many of the above references point out. SICI can be easily eliminated from the diffusive EBM by making some small changes to the heat transport parameterization (North 1984).

Analytic methods are not practical for the more complex models considered later, so we will need to integrate the time-dependent equations numerically to map out their $\phi_i - S_0$ relationships. The basic procedure, which will be repeated for each model, is very similar to that described by Huang and Bowman (1992). We start from a warm, ice-free state and first decrease and then increase S_0 by small increments, allowing the system to re-equilibrate after each perturbation, turning around just before the large ice cap instability threshold. This method finds only the stable equilibria. Numerical results for the simple EBM are plotted in Fig. 1 along with the analytic solutions; the curves differ only in the polar latitudes, where the analytic solution shows an unstable equilibrium but the numerical solution "jumps" over it (this is the effect of SICI).

In anticipation of our later results, note the uniqueness of the ice edge in Fig. 1. Although the EBM supports multiple equilibria in the form of snowball and ice-free solutions, there is never more than one stable solution with a finite ice edge.

b. A note on parameter values

Numerical values for all our calculations are listed in Table 1. Our main results are qualitative and not sensitive to specific parameter choices. For each of the four classes of models presented here, we choose parameter values giving pole-to-equator temperature differences, heat transport profiles, and ice edges in reasonable agreement with the observed climate. Two solutions are shown in each case, taking the outgoing longwave sensitivity B_{out} as either 2.9 or 1.7 W m^{-2} °C^{-1} and tuning A_{out} to give the same ϕ_i for $S_0 = 1367$ W m^{-2}. The B_{out} values are based on linear regression of long-term mean Northern Hemisphere National Centers for Environmental Prediction (NCEP) reanalysis OLR against temperature at 500 and 1000 hPa, respectively. Given that T_a in our models effectively represents both the surface and the midtroposphere (see below), we take these values to be reasonable upper and lower bounds on B_{out}. In every case, smaller B_{out} is associated with enhanced sensitivity of ϕ_i to changes in S_0, analogous to increasing δ in the simple EBM (although the corresponding nondimensional parameter is not so clearly defined in the more complex models considered later).

c. Extension to a simple atmosphere–ocean EBM

Our goal here is to extend (1) to include an explicit atmosphere and ocean, with both thermodynamic and dynamic coupling. The first step is to separate the thermodynamics into two layers, with the lower layer representing the ocean and the upper layer representing the atmosphere. This is the next member of our model hierarchy, which is sketched in Fig. 2. We let the surface (ocean) and atmosphere have temperatures T_s and T_a respectively. The albedo is controlled by T_s [replacing T_a in (2b)]; the outgoing radiation is again given by $A_{\text{out}} + B_{\text{out}}T_a$. Here T_a will be treated as a measure of the free tropospheric temperature, say at 500 hPa. However, we will express it as an equivalent surface air temperature, assuming a constant lapse rate.

The atmosphere will be treated as transparent to solar radiation, so that the net solar flux $\mathcal{A}\mathcal{S}$ is absorbed at the surface. The net heat flux from the surface to the atmosphere is defined as

$$F_{\text{up}} = A_{\text{up}} + B_{\text{up}}(T_s - T_a), \tag{4}$$

with A_{up}, B_{up} constant. This is a crude representation of the net effect of infrared radiation, turbulent heat fluxes, and convection.

To represent atmospheric and oceanic heat transport explicitly, we assume a down-gradient transport in both layers. We can thereby write our atmosphere–ocean EBM (AO-EBM) as a pair of coupled diffusion equations:

$$C_a \frac{\partial T_a}{\partial t} = D_y\left(C_a K_a \frac{\partial T_a}{\partial y}\right) + A_{\text{up}} + B_{\text{up}}(T_s - T_a) - B_{\text{out}}T_a - A_{\text{out}}, \tag{5a}$$

$$C_o \frac{\partial T_s}{\partial t} = D_y\left(C_o K_o \frac{\partial T_s}{\partial y}\right) + \mathcal{A}S - A_{\text{up}} - B_{\text{up}}(T_s - T_a). \tag{5b}$$

Held and Suarez (1974) looked at a similar atmosphere–ocean generalization of the Budyko-type EBM. With constant coefficients, they showed a mathematical equivalence of their AO-EBM to the simple one-layer EBM. Thus, although the extension to two layers may provide a physically more meaningful framework for estimating parameter values, it does not lead to any qualitatively new behavior in the climate. Similarly, although we use the more physically motivated diffusive (Sellers-type) transport, we find that our AO-EBM [(5)] does not yield any qualitatively new behavior when the diffusivities K_a, K_o are constant in latitude.[3] This equivalence of (5) and (1) is confirmed by the results plotted in Fig. 2. Despite the added complexity of the distinct atmosphere and ocean layers with separate heat transport, there is no qualitative change in the ϕ_i–S_0 graph compared to Fig. 1 (these are numerical solutions, so only stable solutions are shown).

A clue as to what is required to endow the EBM with qualitatively new behavior is offered by Lindzen and Farrell (1977): they argue that the stability of the ice edge depends only on the range of latitudes over which a heat transport mechanism is acting to smooth temperature and the efficiency with which it does so. In the real world, the ocean is driven by the wind stress, which varies over subplanetary scales, leading to considerable structure in the ocean's meridional energy transport. In simple EBMs we represent the ocean heat transport as a hemispheric-scale diffusion, which cannot capture the important physics of the gyre scale. In the next section we constrain the ocean in a physically more meaningful way and in doing so, we introduce smaller, more realistic scales to ocean heat transport. This turns out to be crucial to the sensitivity of the ice edge.

3. Ocean heat transport and sea ice

In this section we refine the surface Eq. (5b) of the AO-EBM to account more fully for the separate roles of oceanic transport and ice cover on the energy balance. These issues are most easily understood in an aquaplanet framework with interacting atmosphere, ocean, and sea ice but without land surfaces, as in the coupled model of Marshall et al. (2007), because land ice is constrained less directly than sea ice by sea surface conditions and ocean heat transport. We therefore now focus attention on the representation of sea ice and its interaction with the ocean.

a. Sea ice

Sea ice has three basic properties that are crucial for the large-scale energy balance: it forms where the sea surface temperature reaches the freezing point, it is highly reflective compared to open water, and it insulates the ocean surface from the atmosphere (e.g., Bendtsen 2002). The albedo parameterization in the simple AO-EBM in Fig. 2 captures the first two of these properties, but not the third. With K_o constant everywhere, there is a nonzero ocean heat transport convergence under the ice, which is communicated upward to heat the atmosphere exactly as it would be in the absence of ice.

[3] North (1975b) showed that the diffusive EBM and the Budyko-type EBM are equivalent under a spectral truncation. It can also be shown that the steady-state, constant-K form of (5) is isomorphic with (1) up to a spectral truncation error.

The simplest time-dependent model of sea ice is the ''0-layer'' thermodynamic model of Semtner (1976), which assumes an ice top temperature T_i in balance with the heat fluxes at the surface, the temperature at the base of the ice fixed at freezing T_f, and a linear conductive heat flux through the ice pack: $F_c = \kappa_i(T_f - T_i)/h_i$, where κ_i is constant. The prognostic variable is the ice thickness h_i, evolving in response to imbalances in the energy flux at the top and bottom of the ice pack. This model is an approximation to the detailed thermodynamic model of Maykut and Untersteiner (1971), itself an approximation to the fundamental equations for a two-phase brine–ice mixture or ''mushy layer'' (Feltham et al. 2006). Bendtsen (2002) coupled this type of sea ice model to a zonally averaged atmosphere–ocean EBM.

Focusing on the steady-state response to mean annual forcing, we consider an even simpler limit, in which the ice is a perfect insulator. Setting $\kappa_i = 0$ in the Semtner model effectively means that the ice thickness h_i drops out of the problem, and the existence of ice can be diagnosed directly from the temperatures (as in the EBM). Therefore, if we let T_i be determined by local radiative equilibrium with the atmosphere and assume that the underlying ocean temperature $T_o = T_f$ everywhere under the ice, then the ocean heat transport goes to zero at the ice edge. We represent this limit with a single equation [(5b)] for a single temperature T_s simply by setting $K_o = 0$ and $\mathcal{A} = \mathcal{A}_i$ wherever $T_s < T_f$. The temperature T_s characterizes whichever surface is exposed to the atmosphere—either ocean or ice.[4]

Before proceeding to a more sophisticated ocean model, we note that simply setting $K_o = 0$ poleward of the ice edge but otherwise holding it constant does not generate additional equilibria in the AO-EBM [(5)]. The $\phi_i - S_0$ graph in this case (not shown) is similar to Fig. 2 except that the SICI is absent (there are stable ice edges all the way to the pole). Thus, we conclude that the insulating property of sea ice alone is not sufficient to generate new equilibria in the AO-EBM.

b. Wind-driven gyres and ocean diffusivity

We now develop a simple parameterization for ocean heat transport (denoted $\mathcal{H}_o$) by wind-driven gyres. We consider the heat budget of a homogeneous ocean layer of depth h_m, driven by the zonal mean wind stress τ and exchanging heat with the atmosphere. Physically we might conceptualize this as a horizontally circulating wind-driven mixed layer overlying a motionless abyss with no overturning, in which there is no significant land surface but the ocean is confined to a basin geometry by a thin continental ridge running from pole to equator [the ''ridgeworld'' of Enderton and Marshall (2009)]. In this simple limit we can write the ocean heat transport across zonal sections as

$$\mathcal{H}_o = 2\pi a \cos\phi C_o \overline{v' T_s'}, \tag{6}$$

where v is the meridional flow and $C_o = c_o \rho_o h_m$, where c_o and ρ_o are respectively the specific heat and density of the ocean of depth h_m. We assume here that the transport is dominated by ocean gyres, so that it is well approximated by an interior in Sverdrup balance, with return flow in a western boundary layer. The interior meridional velocity is therefore

$$v_S = -\frac{1}{\beta \rho_o h_m} D_y(\tau), \tag{7}$$

where $\beta = 2\Omega a^{-1}\cos\phi$ is the planetary vorticity gradient, τ is the applied zonal wind stress (assumed to be constant in longitude), and D_y is our divergence operator.[5] We further assume that the temperatures of the interior and western boundary current differ by ΔT, which is a function of latitude only. Then for a western boundary current of fractional width γ, the temperature flux can be written

$$\overline{v' T_s'} = \frac{(1-\gamma)\Delta T}{\beta \rho_o h_m} D_y(\tau). \tag{8}$$

Under these assumptions, the problem of heat transport by ocean gyres reduces to finding a closure for ΔT. The temperature anomaly results from preferential advection in the western boundary, such that it could plausibly depend on the steepness of the meridional temperature gradient. The sign and strength of the advection depend on the sense of the gyre, itself set by the wind curl. In this spirit we choose the following closure:

$$\Delta T = -\mu^* \frac{(a\cos\phi)^2}{\tau_0} D_y(\tau) \frac{\partial T_s}{\partial y}. \tag{9}$$

[4] We continue to take $T_f = -10$°C (the canonical threshold temperature in simple EBMs, based on the mean annual position of the land-based snow line) for ease of comparison with established results. A more appropriate threshold for this sea ice model might be $T_f = -2$°C, roughly the freezing point of seawater. The main results of this paper (in particular, the existence of multiple stable ice edges to be discussed later) are not sensitive to this choice: we have obtained the same qualitative results using $T_f = -2$°C.

[5] Here D_y is used to take the curl of stress τ (more precisely, the vertical component of the curl). This has the same mathematical form as the divergence because τ varies only in latitude.

Here τ_0 is a constant scale value for the stress, and the constant of proportionality μ^* is a dimensionless number, related to the fractional zonal temperature difference across the basin with respect to a given meridional temperature change. In practice μ^* is an adjustable parameter that sets the magnitude of the ocean heat transport (the shape being set by the wind).

With this parameterization [substituting (9) and (8) into (6)] we can write the ocean heat transport in terms of the wind stress curl and temperature gradient thus [absorbing the factor $(1 - \gamma)$ into μ^*]:

$$\mathcal{H}_o = -\frac{2\pi(a\cos\phi)^3 c_o \mu^*}{\beta\tau_0}[D_y(\tau)]^2 \frac{\partial T_s}{\partial y}. \qquad (10)$$

Note that $\mathcal{H}_o$ depends on the square of the wind curl and is thus nonnegative at all latitudes: both the subtropical and subpolar gyres carry heat poleward despite the change in sign of the mass transport because ΔT also changes sign.[6] The dependence of $\mathcal{H}_o$ on the square of the wind curl corresponds to the weak gyre advection and strong temperature-restoring limit of the idealized gyral heat transport problem studied by Wang et al. (1995). An expression very similar to (10) was previously derived by Gallego and Cessi (2000) for heat transport by wind-driven gyres, although their model also includes a constant background diffusivity independent of the wind forcing.

Because we have set $\mathcal{H}_o$ proportional to the temperature gradient, our heat equation once again takes the form of a diffusion equation—in fact, we recover (5b), but with the ocean diffusion coefficient now proportional to the square of the local wind stress curl:

$$K_o = \frac{a^3\cos\phi\mu}{f_0 C_o}[D_y(\tau)]^2, \qquad (11)$$

where we have rewritten the constants using $f_0 = 2\Omega\sin(45^\circ) = (\sqrt{2}\cos\phi)^{-1}\beta a$ and defined a dimensional constant $\mu = (\sqrt{2}\tau_0)^{-1}c_o\mu^*$.

In the next section we find solutions to the AO-EBM (5) with the ocean diffusivity (11) and with $K_o = 0$ in the ice-covered region. This model setup is sketched at the top left of Fig. 3. Note that because the ocean heat equation depends on the product C_oK_o, which is independent of depth h_m, the steady-state solutions are also independent of h_m.

c. Multiple equilibria in the AO-EBM with specified winds

To explore the properties of our new model, let us first suppose that the wind stress is externally specified. The final member of our model hierarchy, to be discussed in the next section, is capable of generating a wind stress interactively in response to the differential heating of the atmosphere. For now, we will simply "borrow" the wind field generated by the interactive model, which is plotted in Fig. 4. It features a broad band of easterlies stretching from the equator to 33° and an even broader and more intense band of westerlies peaking at 64° and extending almost to the pole. We show in the appendix that the surface stress associated with this wind field is subject to a momentum constraint ensuring that its area-weighted global integral is zero. The main disparity between this idealized wind field and the observed time- and zonal-mean zonal wind fields is the position of the westerly maximum, which actually occurs near 50°. Taking the square of the curl of this wind stress to apply our ocean diffusivity parameterization (11) leaves us with two broad regions of enhanced diffusivity centered at 32° and 76°, which we associate with subtropical and subpolar gyres; K_o has minima at the zero curl lines located near 11°, 56°, and 88°. We integrate (5) numerically with this variable K_o but with constant atmospheric diffusivity K_a. We also set $K_o = 0$ poleward of ϕ_i at each time step to set meridional ocean energy transport to zero, thus representing the insulating effect of sea ice.

Figure 3 is analogous to Figs. 1 and 2, giving results for this AO-EBM with fixed winds and insulating sea ice. Parameters are chosen to yield a high-latitude ϕ_i for a realistic value of S_0 (see Table 1). This solution is plotted in detail in the top right of Fig. 3. The ocean heat transport $\mathcal{H}_o$ now exhibits a subhemispheric-scale meridional structure imposed by the wind: there is a primary maximum in the subtropical gyre and a secondary maximum in the subpolar gyre with a minimum in between, at the midlatitude zero curl line.[7]

At bottom right in Fig. 3 is an additional stable solution for the same solar forcing, in which the entire subpolar gyre is frozen over and ϕ_i rests at the zero curl

[6] In the real oceans the gyres contribute to poleward heat transport everywhere except in the equatorial regions, where the circulation is opposite to that of the neighboring subtropical gyres, but there is no corresponding change in sign of ΔT. However, the equatorward heat transport by the equatorial gyres is small and is overwhelmed by the substantial poleward heat transport by wind-driven subtropical cells (see, e.g., Hazeleger et al. 2004; Enderton and Marshall 2009).

[7] It is interesting to note that Enderton and Marshall (2009) find a qualitatively similar bimodal $\mathcal{H}_o$ in coupled GCM simulations in "ridgeworld" geometry, where the ocean circulation is dominated by gyres (see, e.g., their Fig. 10). The 2D wind-driven ocean model of Primeau and Cessi (2001) also generates such a bimodal $\mathcal{H}_o$.

line (and the climate is consequently much colder). This new stable equilibrium state, which has no analog in the simple EBM, is the principal new result of this paper. Its existence is intimately related to the meridional structure imprinted on the ocean heat transport by the wind.

The $\phi_i - S_0$ graphs for this wind-driven model (lower left in Fig. 3) are qualitatively different than those of the constant-diffusivity cases considered earlier: there is a marked asymmetry between the cooling and warming branches due to the new multiple equilibrium regime. In the cooling phase, the ice edge advances gradually over the subpolar gyre as S_0 is reduced. In the warming phase, ϕ_i remains at the zero curl line over a wide range of S_0 values until a threshold is reached near 1400 W m^{-2}, which causes a complete melting of the subpolar ice cover. An additional, similar multiple equilibrium regime and threshold at higher S_0 values is associated with the zero curl line near the pole.

These results can be understood as follows. At steady state, $\mathcal{H}_o$ must go smoothly to zero at ϕ_i; this requires either zero wind curl or zero temperature gradient [see Eq. (10)]. Thus it is possible for the ice edge to rest in the interior of a gyre, but only if T_s flattens out at T_f just equatorward of ϕ_i. In contrast, if the ice edge rests at a zero curl line, the system can support ocean temperatures above freezing just equatorward of ϕ_i (this can be seen in Fig. 3). This icy solution collapses when the temperature just poleward of ϕ_i (set by radiative balance with the atmosphere) rises above T_f.

The cooling branch of the $\phi_i - S_0$ curves differ in important ways from the constant-diffusivity cases, even disregarding the existence of the multiple equilibria. Their slopes are highly variable—the ice is much more sensitive to changes in the heat budget when the edge is located in the interior of a gyre (i.e., a latitude of efficient ocean heat transport). On the other hand, ϕ_i is quite insensitive to changes in the heat budget when it is located near a zero curl line (i.e., at a latitude characterized by inefficient ocean heat transport). This is a somewhat more general argument than the wind-curl dependence posited here. It implies that the regions of low ocean transport efficiency are the most likely places for the ice edge to rest.

There are no qualitative differences between the small B_{out} and large B_{out} versions of the model in Fig. 3. The multiple equilibrium regime spans a larger range of S_0 values for larger B_{out}. We emphasize that the new equilibrium is not an expression of SICI; here we have the coexistence of two finite ice caps of different sizes, and the underlying physical mechanism is rather different than the SICI mechanism outlined in section 2. This model does not have a minimum stable ice cap size (Fig. 3 shows that stable small polar ice caps are possible). Furthermore, in the new cold solution in Fig. 3 the ice edge is slaved to the position of the midlatitude zero wind curl line because there is no ocean heat transport across this line. Thus, the ice edge is fixed at a particular latitude (about 55°) for a wide range of solar forcing, unlike the multiple equilibria generated by SICI in the simple EBM (Figs. 1 and 2).

In the next section we introduce a dynamical process into the EBM in order to calculate τ interactively. As we will see, this fully coupled model generates essentially the same multiple equilibrium behavior discussed above, but without the need to externally specify a wind stress forcing.

4. An energy-momentum balance model

We now develop an extension to the atmospheric EBM framework that allows us to simultaneously represent poleward heat transport by synoptic eddies and their associated angular momentum transport that acts to maintain the surface wind stress. In so doing, and by coupling this atmosphere to the wind-driven ocean developed in the previous section, we arrive at a simple system of equations in which the atmosphere and ocean are coupled together both dynamically and thermodynamically. This final member of our model hierarchy is illustrated in the top left of Fig. 4. In it we represent the transfer of angular momentum by Reynold stresses transporting westerly momentum out of the tropics in to midlatitudes, inducing tropical trade winds and midlatitude surface westerlies. To represent this angular momentum transfer,[8] we hypothesize that atmospheric eddies mix potential vorticity (PV) subject to a global angular momentum constraint—that is, eddies should not generate any net momentum but only redistribute it.

a. Formulation

We exploit an idea first developed by Green (1970), who, using a quasigeostrophic (QG) beta-plane framework, represented the eddy forcing of the zonal mean wind through a diffusive parameterization on the QG potential vorticity (QGPV). By assuming a plausible form for the baroclinicity of the atmosphere, Green (1970) and White (1977) were able to derive analytic solutions for the zonal mean surface wind, obtaining the familiar tropical easterlies, midlatitude westerlies, and polar easterlies. Subsequently, Wu and White (1986)

[8] As has been known since the work of Jeffreys (1926), angular momentum transport by synoptic eddies cannot be represented as a diffusive process because westerly momentum is transported up the mean gradient to maintain the midlatitude westerly jet. Instead we choose to mix PV, following Green (1970).

demonstrated the extension of Green's idea to the sphere, using a two-level QGPV framework, and showed that the existence of polar easterlies is rather sensitive to model details. Here we couple the two-level, spherical QGPV system to an energy balance calculation, such that the baroclinicity and the surface wind are predicted simultaneously. Essentially we diffuse PV in two atmospheric layers, rather than, as in the previous section, diffusing temperature in a single layer. Similar models were previously considered by Cessi (2000) and Gallego and Cessi (2000) in Cartesian beta-plane geometry, and by Primeau and Cessi (2001) in spherical geometry. The two-level approach was also used by Marshall (1981) for a zonally averaged ocean channel model. The details of the derivation are laid out in the appendix. Briefly, the two-level QGPV equations are zonally averaged, and the eddy flux terms are closed by

$$\overline{v_i' q_i'} = -K_i \frac{\partial q_i}{\partial y}, \quad \text{for} \quad i = u, l, \tag{12}$$

where q is the zonal-mean PV, K is a diffusivity, and the subscripts u and l refer respectively to the upper and lower atmospheric levels. The diffusion coefficients are assumed to peak in the midlatitudes and to go to zero at the equator and pole. Their relative magnitudes are related by exploiting an angular momentum constraint that states that the surface stress, when integrated over the globe, identically vanishes at equilibrium. This leaves a single scalar parameter to be chosen to control the absolute magnitudes of the diffusivities.

Following the notation of the previous section, τ is the stress of the wind acting on the ocean. With the diffusive closure (12) for PV, we can then write the time-dependent two-level PV system as

$$\frac{\partial}{\partial t} q_u = D_y \left(K_u \frac{\partial q_u}{\partial y} \right) - \frac{R}{C_a L_d^2 f_0} \dot{Q}, \tag{13a}$$

$$\frac{\partial}{\partial t} q_l = D_y \left(K_l \frac{\partial q_l}{\partial y} \right) + \frac{R}{C_a L_d^2 f_0} \dot{Q} + \frac{2g}{p_0} D_y(\tau), \tag{13b}$$

where $\dot{Q}$ is the diabatic heating rate in watts per square meter, R is the gas constant for dry air, and L_d is the deformation radius.

The heating is specified in the same way as in the AO-EBM, so that $\dot{Q} = A_{\text{up}} + B_{\text{up}}(T_s - T_a) - A_{\text{out}} - B_{\text{out}} T_a$. The system (13) is solved by expressing the temperature and stress in terms of the winds, which are related to the PV gradients by

$$\frac{\partial}{\partial y} q_u = \beta - \frac{\partial}{\partial y} [D_y(u_u)] + \frac{u_d}{L_d^2} \quad \text{and} \tag{14a}$$

$$\frac{\partial}{\partial y} q_l = \beta - \frac{\partial}{\partial y} [D_y(u_l)] - \frac{u_d}{L_d^2}, \tag{14b}$$

where u_u and u_l are the upper- and lower-level zonal mean winds and $u_d = u_u - u_l$ is the shear. The winds are obtained by inversion of (14) subject to $u = 0$ at $\phi = 0°$, 90°. We use a linear drag law to relate the stress [last term in (13b)] to the winds, and the imposed momentum constraint on the PV diffusion ensures that τ integrates to zero globally at equilibrium. The atmospheric temperature T_a is set by the wind shear from the thermal wind balance up to a constant of integration. We solve for the global mean temperature by invoking global energy conservation:

$$C_a \frac{d}{dt} \langle T_a \rangle = \langle \dot{Q} \rangle, \tag{15}$$

where the angle brackets represent an area-weighted global mean $\langle h \rangle = \int_0^{\pi/2} h \cos\phi \, d\phi$.

Our atmosphere thus consists of two coupled diffusion equations [(13)] for PV with thermal, mechanical, and eddy forcing calculated from winds and temperature, along with the prognostic equation (15) for global mean temperature. The ocean is represented by the heat diffusion equation (5b) with the wind-driven diffusivity (11), which is now coupled to the atmosphere thermodynamically through the heat exchange $A_{\text{up}} + B_{\text{up}}(T_s - T_a)$ and mechanically through the stress τ. We thus have a system of three prognostic PDEs and one prognostic ODE that can be integrated numerically by a simple timestepping procedure, with inversion of the QGPV according to (14) between each time step. We refer to this system as the energy-momentum balance model, or EMomBM.[9] The model is readily spun up to steady state on a laptop.

Our EMomBM is similar to the zonally averaged wind-driven model discussed by Gallego and Cessi (2000), which also couples together Green's model for atmospheric eddy momentum fluxes with an energy balance calculation and a simple description of wind-driven ocean gyres. Our model differs from this earlier work in the inclusion of sea ice and spherical geometry and the lack of an explicit delay time for the wind forcing of the ocean (in our model gyres adjust instantaneously to changes in wind forcing, implying very fast Rossby wave speeds). These differences reflect the very different intended applications of the two models. We are primarily interested in the role of the wind-driven ocean circulation in setting sea ice extent and thus,

[9] Not to be confused with an energy–moisture balance model, which is sometimes abbreviated EMBM in the literature.

through the nonlinear albedo feedback, allowing for multiple stable equilibria (as we show in the next section). Gallego and Cessi (2000), on the other hand, focus on coupled modes of variability in the midlatitude atmosphere–ocean system, and their model exhibits decadal-scale oscillatory solutions due to the finite cross-basin Rossby wave transit time. A more comprehensive model would include both sea ice and a finite delay time for the gyres; whether such a model would exhibit multiple oscillatory solutions is left as an open question.

b. Multiple equilibria in the EMomBM

Parameters for EMomBM are listed in Table 1 (see the appendix for further definitions). Values were chosen to give roughly the same ice edge and heat transports as found for the fixed-wind AO-EBM in Fig. 3. The maximum value of atmospheric diffusivity is 6×10^6 m^2 s^{-1}, which occurs in the midlatitude lower troposphere; this is consistent with a simple scaling in terms of eddy mixing lengths and wind speeds.

The EMomBM exhibits multiple equilibria that are quite similar to that found in the fixed-wind model, as illustrated by the two solutions plotted at top right and bottom right of Fig. 4. The similarity to the solutions plotted in Fig. 3 demonstrates two things: the two-level QGPV diffusion equations [(13)] can reproduce the temperature field predicted by the one-level heat diffusion equation [(5a)], and the surface wind stress generated by the EMomBM is quite robust (the winds in the upper and lower panels look nearly the same, despite substantial changes in albedo and temperature).

Because the winds do not vary much, the ϕ_i–S_0 graph (lower left in Fig. 4) is quite similar to its fixed-wind counterpart in Fig. 3. Thus our earlier discussion on the multiple equilibrium regimes applies equally to this EMomBM. There are, however, some differences from the fixed-wind case: the ranges of S_0 for which the multiple equilibria exist are smaller, and the jump in ϕ_i as the system warms past its threshold is more modest. These differences are related to subtle shifts in the position and magnitude of the wind stress, and thus the shape of K_o, that occur in response to changes in ϕ_i (and thus the differential heating of the atmosphere). Apparently the feedback among ice, wind, and ocean heat transport in the EMomBM acts to destabilize the cold solution somewhat. Paradoxically, this may actually increase the likelihood of abrupt changes in the system under variable forcing because smaller variations in the heat budget are required to span the hysteresis loop.

Here we briefly explore the climatic implications of the hysteresis loop in the EMomBM. The ϕ_i–S_0 graphs suggest that an external forcing that raises and lowers the energy budget of the climate system has the potential to generate asymmetric warming and cooling, without driving the climate to snowball extremes. To make this idea explicit, we integrate the EMomBM with imposed time-dependent sinusoidal variations in A_{out} (setting the global mean longwave cooling) while holding S_0 fixed.[10]

The time history of the forcing and of the response for three different runs is shown in Fig. 5. We impose A_{out} variations on the order of 10 W m^{-2}, which is roughly equivalent to a threefold variation in CO_2 concentration, based on the classic radiative transfer calculations of Manabe and Wetherald (1967), holding relative humidity fixed. For these integrations we have set the ocean heat capacity to $C_o = 4 \times 10^8$ J m^{-2} °C^{-1}, corresponding to an ocean mixed layer depth of about 90 m. The time scale of the forcing (2000 yr) is arbitrary but long compared to the equilibration time of the system (roughly 10 yr).

We show in Fig. 5 that by making small changes in the amplitude of A_{out} variations (± 1 W m^{-2}), we can generate very different climate variability in the EMomBM. Each of the three runs is initialized from a warm state and cools gradually in response to the increase in longwave emission. In one case (dashed curve) the climate varies linearly with the forcing, with the ice expanding and melting back gradually through three forcing cycles. The maximum value of A_{out} (first reached after 1000 yr) is not large enough in this case for ϕ_i to reach the midlatitude zero curl line. A second case (solid curve) does get cold enough to freeze over the entire subpolar gyre, and ϕ_i consequently remains fixed at the zero curl line while the ''greenhouse warming'' increases (A_{out} decreases) until the system warms past the melting threshold. The resulting climate variations have a sawtooth shape illustrating a distinct asymmetry: gradual cooling and abrupt warming. The third case (dashed–dotted curve) has a slightly greater minimum A_{out} value, such that the abrupt warming threshold is never reached. In this case, the climate cools gradually during the first cycle, and ϕ_i reaches the zero curl line and never recovers. As a result, the global mean air temperature is some 6°C colder than the other two runs at the warmest point in the cycle.

5. Conclusions

The main goal of this paper was to demonstrate the existence of an additional stable equilibrium climate

[10] Here we choose to vary A_{out} partly to explore a different parameter sensitivity in the model, but we do so also because A_{out} is a better analog to the effects of greenhouse gas concentration than S_0, since S_0 projects both onto the global mean energy budget and its pole-to-equator gradient.

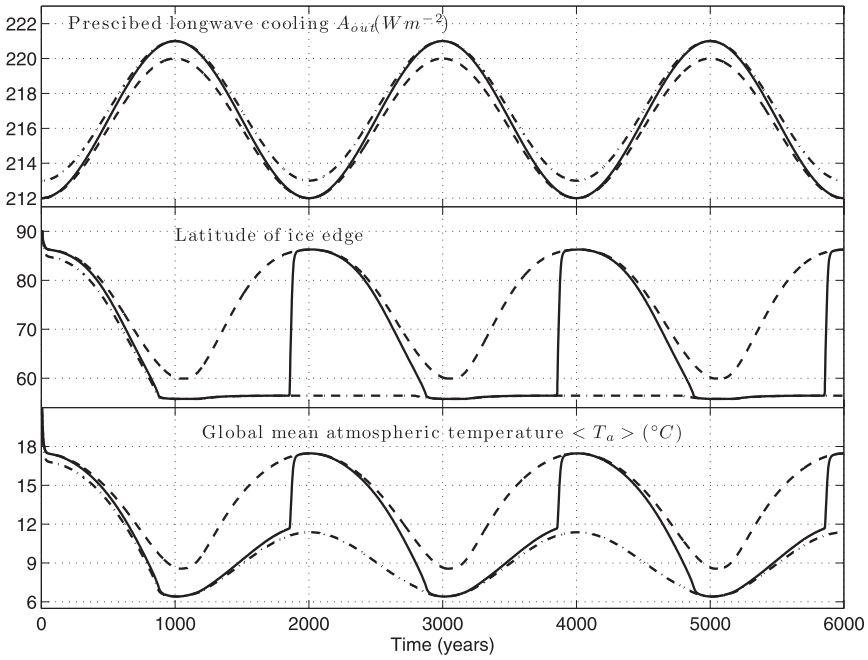

FIG. 5. A time-dependent case with sinusoidally varying forcing. (top) Three separate integrations of the EMomBM are initialized from a warm, ice-free state and forced by sinusoidal variations of the longwave cooling constant A_{out} over 2000-yr periods. The resulting (middle) ice edge and (bottom) global mean atmospheric temperature. The three runs each produce very different climate variations as a result of small differences in the amplitude of the thermal forcing. Parameters are as in Fig. 4 (with $B_{\text{out}} = 1.7$ W m^{-2} °C^{-1}), but with C_o set to a more realistic value of 4×10^8 J m^{-2} °C^{-1}, giving an adjustment time of about 10 yr for the system (short compared to the time scale of the forcing).

state in an extension of the well-known energy balance model. The new equilibrium state features a midlatitude ice edge and has no analog in the simple EBM. It coexists with the warmer, small ice cap solution and the very cold ''snowball'' solution found in the simple EBM. The minimal new physics required to support this new equilibrium are twofold: the ocean heat transport must have some latitudinal structure with a minimum in midlatitudes, and the sea ice must insulate the ocean from the atmosphere (which requires that the ocean heat transport go to zero at the ice edge at steady state).

We have described a new energy-momentum balance model, at the heart of which is two new features. For the ocean, we have considered wind-driven gyres in Sverdrup balance whose meridional energy transport is represented by a heat equation in which the diffusion coefficient is set proportional to the square of the curl of the wind stress. Thus, the meridional scales of the wind forcing are imprinted on the ocean, and in particular, $\mathcal{H}_o$ has a minimum within the midlatitude band of westerlies. We have modeled the atmosphere as a two-level quasigeostrophic system in order to solve simultaneously for the energy and angular momentum balance in the simplest possible way. The surface stress generated by the QG atmosphere is used to drive the ocean. The two fluids are thus coupled together both thermodynamically and mechanically. This model responds to an imposed differential heating by fluxing heat poleward in the atmosphere while simultaneously generating a midlatitude westerly wind band that drives subtropical and subpolar ocean gyres, both of which also carry heat poleward (so long as they are not frozen over).

Our results with the fixed-wind model indicate that the mechanical coupling between atmosphere and ocean in the EMomBM is not required to support the new equilibrium state; heat diffusion with K_o varying in latitude but fixed in time is sufficient for the new behavior. However, we feel that the EMomBM is interesting in its own right. It is one of the most compact expressions of the simultaneous conservation of heat and angular momentum in the climate system. With only a modest increase in computation over the simplest EBM, we solve for a quantity (wind stress) that is fundamental to atmosphere–ocean coupling. This EMomBM may therefore help fill in a gap in our spectrum of climate models.

The specific arguments laid out in section 3 linking $\mathcal{H}_o$ and τ are somewhat tenuous; we do not claim that this is the most useful coarse-grained description of a wind-driven ocean. The larger point seems to be that the scales of motion in the ocean, unlike the atmosphere, are such that the heat transport mechanisms may operate over subhemispheric scales, and this can have profound implications on the equilibrium position of the ice edge. We noted in section 3 that, even ignoring the existence of multiple equilibria, the sensitivity of the ice edge to changes in the heat budget varies considerably depending on the proximity of the ice edge to a region of minimum ocean heat transport efficiency (i.e., minimum K_o). The maintenance of the ice edge in a region of high K_o therefore requires a rather delicate balance of forcing; we expect that in a noisy, eddying climate system the ice edge would spend much more time near minima in K_o.

Finally, we emphasize that the hysteresis loop in our new model, with its abrupt warmings and gradual coolings, is generated in a coupled atmosphere–ocean–ice system with a purely wind-driven ocean; we do not consider any ocean overturning or thermohaline effects. This suggests a need for a more careful consideration of the role of winds in the dynamics of past climate changes—in particular, the abrupt warmings known to have occurred repeatedly throughout the last ice age.

Acknowledgments. We thank Jean-Michel Campin for advice on the numerical algorithms, David Ferreira for an insightful review of an early draft of this manuscript, and two anonymous reviewers for helpful comments. Brian Rose received support from MIT's Climate Modeling Initiative and NSF Ocean Sciences.

APPENDIX

Derivation of the Atmospheric Model

The model is based on the dry two-level QGPV equations first derived on a β plane by Phillips (1956). The extension of QG theory to spherical geometry is discussed in detail by Mak (1991). Here we adopt the form used by Marshall and Molteni (1993), retaining the full latitude dependence of the Coriolis parameter $f = 2\Omega \sin\phi$ in the horizontal advection terms but using a constant value f_0 in the stretching term and the thermal wind equation. Let QGPV be defined in pressure coordinates as

$$q = \nabla^2\psi + f + f_0^2 \frac{\partial}{\partial p}\left(\sigma^{-1}\frac{\partial \psi}{\partial p}\right), \tag{A1}$$

which evolves according to

$$\left(\frac{\partial}{\partial t} + \mathbf{v}_\psi \cdot \nabla\right) q = g\frac{\partial}{\partial p}(\hat{k}\cdot\nabla\times\tau) - f_0\frac{\partial}{\partial p}\left(\frac{RJ}{\sigma p}\right), \tag{A2}$$

where ψ is the geostrophic streamfunction, $\mathbf{v}_\psi$ is the geostrophic advecting velocity, σ is the static stability (assumed to a function of pressure only), τ is a mechanical stress, and J is a diabatic heating rate in degrees Celsius per second.

We now take a zonal average of (A2) (resulting in the eddy PV flux $\overline{v'q'}$ appearing as a forcing on the zonal mean) and divide the atmosphere into two equal mass layers. We assume that the bottom boundary at $p_0 =$ 1000 hPa is the only significant source of mechanical stress on the atmosphere, which we will express in terms of the equal and opposite stress τ of the atmosphere on the surface. The diabatic heating is applied at the interface between the layers (500 hPa). Discretizing the zonal mean of (A2) by a vertical finite difference yields the following pair of equations for the zonal mean PV in the upper and lower layers:

$$\frac{\partial}{\partial t} q_u = -D_y(\overline{v_u' q_u'}) - \frac{R}{C_a L_d^2 f_0}\dot{Q}, \quad \text{and} \tag{A3a}$$

$$\frac{\partial}{\partial t} q_l = -D_y(\overline{v_l' q_l'}) + \frac{R}{C_a L_d^2 f_0}\dot{Q} + \frac{2g}{p_0} D_y(\tau), \tag{A3b}$$

where $\dot{Q} = C_a J$ is the column-integrated diabatic heating in watts per square meter and D_y is the meridional divergence operator as used throughout this paper. We have also expressed the stratification in terms of a deformation radius $L_d = \Delta p f_0^{-1}\sigma^{1/2}$, which is held constant.

The flow is calculated at each time step by inversion of the zonal mean PV gradients (14), subject to boundary conditions $u_u = u_l = 0$ at $\phi = 0°, 90°$ (an equatorial wall). The system is closed by expressing PV fluxes, heating, and stress in terms of the winds.

The global momentum conservation constraint can be expressed on the hemisphere as

$$\int_0^{\pi/2} (\overline{v_u' q_u'} + \overline{v_l' q_l'}) \cos\phi \, d\phi = 0, \tag{A4}$$

implying a steady-state balance

$$\int_0^{\pi/2} \tau \cos\phi \, d\phi = 0. \tag{A5}$$

Following Green (1970) and White (1977), we close the eddy flux terms in the PV equation by setting them to be down the mean PV gradients, according to (12). The values of the diffusion coefficients K_u, K_l are thus constrained by (A4). More details can be found in Marshall

(1981) for a two-layer ocean channel model with parameterized geostrophic eddies. We use Marshall's assumption of a separable form for the coefficients:

$$K_i = k_i \frac{|u_d|}{|u_d|_{\max}}, \quad \text{for} \quad i = u, l, \tag{A6}$$

where k_u, k_l are constants. Thus, eddy fluxes are concentrated in the region of maximum baroclinicity in midlatitudes and go to zero at the equator and pole. Substitution of (A6) into the integral constraint (A4) leads to the condition

$$k_u \int_0^{\pi/2} \frac{\partial q_u}{\partial y} |u_d| \cos\phi \, d\phi = -k_l \int_0^{\pi/2} \frac{\partial q_l}{\partial y} |u_d| \cos\phi \, d\phi. \tag{A7}$$

We fix $k_l = 6 \times 10^6 \text{ m}^2 \text{ s}^{-1}$ and compute k_u from (A7) at each time step. This ensures that the parameterized eddies do not exert a net torque but only redistribute momentum.

Plugging (12) into (A3), the PV equations take the form of diffusion equations (13). These equations are coupled together through the heating term and the dynamical constraint (A7), which sets the relative magnitudes of the diffusivities.

The bottom stress is modeled as a linear drag acting on the wind extrapolated down to the surface, following Phillips (1956):

$$\tau = \epsilon \left(\frac{3}{2} u_l - \frac{1}{2} u_u \right), \tag{A8}$$

where ϵ is a constant and $p_0(g\epsilon)^{-1}$ defines a frictional damping time.

The thermal wind relation for this model can be written

$$\frac{\partial T_a}{\partial y} = -\frac{f_0}{R} u_d. \tag{A9}$$

The temperature T_a is dynamically related to the tilt of the interface between the layers and is thus best thought of as a measure of the midtropospheric temperature, just as in the AO-EBM introduced in section 2. However, the dynamics depend only on its slope and not its magnitude, and all the heating terms are linear, so we can continue to express T_a as an equivalent surface air temperature. The heating $\dot{Q}$ is calculated from T_a and T_s as described in the text.

REFERENCES

Bendtsen, J., 2002: Climate sensitivity to changes in solar insolation in a simple coupled climate model. *Climate Dyn.,* **18,** 595–609.

Bitz, C., M. Holland, E. Hunke, and R. Moritz, 2005: Maintenance of the sea-ice edge. *J. Climate,* **18,** 2903–2921.

Budyko, M., 1969: The effect of solar radiation variations on the climate of the earth. *Tellus,* **21,** 611–619.

Cahalan, R. F., and G. R. North, 1979: A stability theorem for energy-balance climate models. *J. Atmos. Sci.,* **36,** 1178–1188.

Cessi, P., 2000: Thermal feedback on wind stress as a contributing cause of climate variability. *J. Climate,* **13,** 232–244.

Donnadieu, Y., G. Ramstein, F. Fluteau, D. Roche, and A. Ganopolski, 2004: The impact of atmospheric and oceanic heat transports on the sea-ice-albedo instability during the Neoproterozoic. *Climate Dyn.,* **22,** 293–306.

Enderton, D., and J. Marshall, 2009: Explorations of atmosphere–ocean–ice climates on an aquaplanet and their meridional energy transports. *J. Atmos. Sci.,* **66,** 1593–1611.

Feltham, D., N. Untersteiner, J. Wettlaufer, and M. Worster, 2006: Sea ice is a mushy layer. *Geophys. Res. Lett.,* **33,** L14501, doi:10.1029/2006GL026290.

Gallego, B., and P. Cessi, 2000: Exchanges of heat and momentum between the atmosphere and the ocean: A minimal model of decadal oscillations. *Climate Dyn.,* **16,** 479–489.

Green, J., 1970: Transfer properties of the large-scale eddies and the general circulation of the atmosphere. *Quart. J. Roy. Meteor. Soc.,* **96,** 157–185.

Hazeleger, W., R. Seager, M. A. Cane, and N. H. Naik, 2004: How can tropical Pacific Ocean heat transport vary? *J. Phys. Oceanogr.,* **34,** 320–333.

Held, I. M., and M. J. Suarez, 1974: Simple albedo feedback models of the icecaps. *Tellus,* **26,** 613–629.

Huang, J., and K. P. Bowman, 1992: The small ice cap instability in seasonal energy balance models. *Climate Dyn.,* **7,** 205–215.

Jayne, S. R., and J. Marotzke, 1999: A destabilizing thermohaline circulation–atmosphere–sea ice feedback. *J. Climate,* **12,** 642–651.

Jeffreys, H., 1926: On the dynamics of geostrophic winds. *Quart. J. Roy. Meteor. Soc.,* **52,** 85–104.

Klinger, B. A., 1996: A kinematic model of wind-driven meridional heat transport. *J. Phys. Oceanogr.,* **26,** 131–135.

——, and J. Marotzke, 2000: Meridional heat transport by the subtropical cell. *J. Phys. Oceanogr.,* **30,** 696–705.

Langen, P. L., and V. A. Alexeev, 2004: Multiple equilibria and asymmetric climates in the CCM3 coupled to an oceanic mixed layer with thermodynamic sea ice. *Geophys. Res. Lett.,* **31,** L04201, doi:10.1029/2003GL019039.

Lee, W.-H., and G. R. North, 1995: Small ice cap instability in the presence of fluctuations. *Climate Dyn.,* **11,** 242–246.

Lewis, J. P., A. J. Weaver, S. T. Johnston, and M. Eby, 2003: Neoproterozoic "snowball Earth": Dynamic sea ice over a quiescent ocean. *Paleoceanography,* **18,** 1092, doi:10.1029/2003PA000926.

Lindzen, R. S., and B. Farrell, 1977: Some realistic modifications of simple climate models. *J. Atmos. Sci.,* **34,** 1487–1501.

——, and ——, 1980: The role of polar regions in global climate, and a new parameterization of global heat transport. *Mon. Wea. Rev.,* **108,** 2064–2079.

Mak, M., 1991: Influences of the earth's sphericity in the quasi-geostrophic theory. *J. Meteor. Soc. Japan,* **69,** 497–511.

Manabe, S., and R. T. Wetherald, 1967: Thermal equilibrium of the atmosphere with a given distribution of relative humidity. *J. Atmos. Sci.,* **24,** 241–259.

Maqueda, M. A. M., A. Willmott, J. Bamber, and M. Darby, 1998: An investigation of the small ice cap instability in the Southern Hemisphere with a coupled atmosphere–sea ice–ocean–terrestrial ice model. *Climate Dyn.,* **14,** 329–352.

Marshall, J. C., 1981: On the parameterization of geostrophic eddies in the ocean. *J. Phys. Oceanogr.,* **11,** 257–271.

——, and F. Molteni, 1993: Toward a dynamical understanding of planetary-scale flow regimes. *J. Atmos. Sci.,* **50,** 1792–1818.

——, D. Ferreira, J.-M. Campin, and D. Enderton, 2007: Mean climate and variability of the atmosphere and ocean on an aquaplanet. *J. Atmos. Sci.,* **64,** 4270–4286.

Matteucci, G., 1993: Multiple equilibria in a zonal energy balance climate model: The thin ice cap instability. *J. Geophys. Res.,* **98D,** 18 515–18 526.

Maykut, G. A., and N. Untersteiner, 1971: Some results from a time-dependent thermodynamic model of sea ice. *J. Geophys. Res.,* **76,** 1550–1575.

Nakamura, M., 1996: Effects of ice albedo and runoff feedbacks on the thermohaline circulation. *J. Climate,* **9,** 1783–1794.

North, G. R., 1975a: Analytical solution to a simple climate model with diffusive heat transport. *J. Atmos. Sci.,* **32,** 1301–1307.

——, 1975b: Theory of energy-balance climate models. *J. Atmos. Sci.,* **32,** 2033–2043.

——, 1984: The small ice cap instability in diffusive climate models. *J. Atmos. Sci.,* **41,** 3390–3395.

——, R. F. Cahalan, and J. A. Coakley, 1981: Energy balance climate models. *Rev. Geophys. Space Phys.,* **19,** 91–121.

Phillips, N. A., 1956: The general circulation of the atmosphere: A numerical experiment. *Quart. J. Roy. Meteor. Soc.,* **82,** 123–164.

Poulsen, C., and R. Jacob, 2004: Factors that inhibit snowball Earth simulation. *Paleoceanography,* **19,** PA4021, doi:10.1029/2004PA001056.

——, R. T. Pierrehumbert, and R. Jacob, 2001: Impact of ocean dynamics on the simulation of the Neoproterozoic ''snowball Earth.'' *Geophys. Res. Lett.,* **28,** 1575–1578.

Primeau, F., and P. Cessi, 2001: Coupling between wind-driven currents and midlatitude storm tracks. *J. Climate,* **14,** 1243–1261.

Sellers, W. D., 1969: A global climatic model based on the energy balance of the earth–atmosphere system. *J. Appl. Meteor.,* **8,** 392–400.

Semtner, A. J., 1976: A model for the thermodynamic growth of sea ice in numerical investigations of climate. *J. Phys. Oceanogr.,* **6,** 379–389.

Stone, P. H., 1978: Constraints on dynamical transports of energy on a spherical planet. *Dyn. Atmos. Oceans,* **2,** 123–139.

Wang, X., P. H. Stone, and J. Marotzke, 1995: Poleward heat transport in a barotropic ocean model. *J. Phys. Oceanogr.,* **25,** 256–265.

White, A., 1977: The surface flow in a statistical climate model—A test of a parameterization of large-scale momentum fluxes. *Quart. J. Roy. Meteor. Soc.,* **103,** 93–119.

Wu, G.-X., and A. White, 1986: A further study of the surface zonal flow predicted by an eddy flux parametrization scheme. *Quart. J. Roy. Meteor. Soc.,* **112,** 1041–1056.

Yang, J., and J. D. Neelin, 1993: Sea-ice interaction with the thermohaline circulation. *Geophys. Res. Lett.,* **20,** 217–220.

——, and ——, 1997: Decadal variability in coupled sea-ice–thermohaline circulation systems. *J. Climate,* **10,** 3059–3076.